



A novel process of deep drawing based on electro-permanent magnet combined segmental blank holder technique

Hongsheng Zhang^{1,2} · Siji Qin¹

Received: 24 May 2021 / Accepted: 20 August 2021 / Published online: 19 October 2021
© The Author(s), under exclusive licence to Springer-Verlag London Ltd., part of Springer Nature 2021

Abstract

A new electro-permanent magnet combined blank holder technique has been developed by using permanent magnetic force to supply the blank holding force (BHF) for sheet metal deep drawing. In this work, the workability of the designed magnetic circuits was simulated and tested. A series of numerical simulations and experiments have also demonstrated its ability to overcome temperature rise and provide sufficient magnetic force. The advantages and availability of the combined blank holder technique were expatiated by theoretical derivation, and analyzed by FE stress analysis. The feasibility and effectiveness of the new blank holder method have been proven by a series of experiments for deep drawing a workpiece of 08Al with a diameter of 220 mm. With the segmental blank holder, the flange wrinkling is demonstrated to be suppressed well than using the single blank holder. Also, experimental results corroborated that current is only instantaneously imposed when switching magnetic force state, and not at other times.

Keywords Deep drawing · Electro-permanent magnet blank holder · Blank holder force · Magnetic force

1 Introduction

The failures of drawn parts during the deep drawing process are often in the form of wrinkling or cracking. Wrinkling can occur at the flange when the in-plane compressive stress is excessive. Meanwhile, cracking will occur in the formed part under excessive tension stress. Blank holder force (BHF) is the pressing force applied on the flange of drawn part to control material flow during the deep drawing process [1]. In all variable parameters, BHF has a significant influence on suppressing forming defects. Therefore, the determination and control of BHF are important for deep drawing [2, 3].

Over the past few decades, numerous researches focused on the applications and controls of BHF. To improve the formability of sheet metal, some advanced blank holder methods and BHF control techniques were proposed. The closed-loop control method was used in the forming process

to realize the real-time control of BHF [4]. Endelt [5] designed a novel closed-loop controller for a nonlinear system of deep drawing, by which the distribution of BHF can be adjusted to improve the stability of deep drawing. Cheng [6] introduced a mechanical press with the double-axis servo system, which can obtain higher quality products than conventional presses. Modi [7] developed the variable BHF technique using a hydro-forming setup for the deep drawing of the square box. Zhou [8] studied the effect of deep drawing using hydroforming for double-layer sheets. Based on a programmable hydraulic cushion mounted on the press, Siegert [9] proposed the concept of segmented blank holder for generating distributed BHF at every corner. Similarly, recent studies also focused on the use of electro-hydraulic load sensing [10] and electro-mechanical die cushion [11, 12], respectively. Furthermore, the forming quality and accuracy can be improved by integrating the composite elastic cushion with multipoint forming technology [13].

The general sources of BHF mentioned above are mechanical press, hydraulics device, electro-hydraulic, and electro-mechanical cushion. In essence, BHF needs to be balanced by the blank holder counterforce, no matter BHF is provided by conventional press or hydraulics system.

Recently and differently, the electromagnetic blank holder techniques have been extensively researched. Some

✉ Siji Qin
plastics@ysu.edu.cn

¹ School of Mechanical Engineering, Yanshan University, 438 West of Hebei Avenue, Qinhuangdao 066004, China

² School of Environment and Chemical Engineering, Yanshan University, Qinhuangdao 066004, China

electromagnetic techniques [14, 15] can apply BHF by use of the magnetic attractive force, and others used the electromagnetic repulsive force [16, 17]. The electromagnetic blank holder technique has some obvious advantages, such as can apply BHF independently without counterforce, and the application time of changing BHF is always extremely short. However, this technique has some distinct disadvantages, since the existence of BHF depends on whether the current is incoming. For example, even if the pulsed electromagnetic system [18] is the most energy-saving blank holder technique, the energies consumed by the sustained current for maintaining BHF during deep drawing are very huge. Meanwhile, since all energies released by the current are in the form of heat during deep drawing, the reduction of temperature rises in the electromagnetic forming is a big problem [19].

In this study, a novel electro-permanent magnet combined blank holder (ECBH) technique for the square box is proposed, which is installed on the conventional press. Unlike the electromagnetic technique, the ECBH technique does not require a continuous current for applying BHF during deep drawing, because the coupling magnetic field is generated by the permanent magnets. Moreover, appropriate BHF with different values can be applied to every circumferential and radial flange region independently and effectively. The theoretical formula of the ECBH technique has been deduced in this paper, and the feasibility and effectiveness of the novel system have been verified through both the numerical simulations and experiments.

2 Design of ECBH system and deep drawing process

In this investigation, a novel ECBH for the conventional deep drawing process has been designed. The equipment shown in

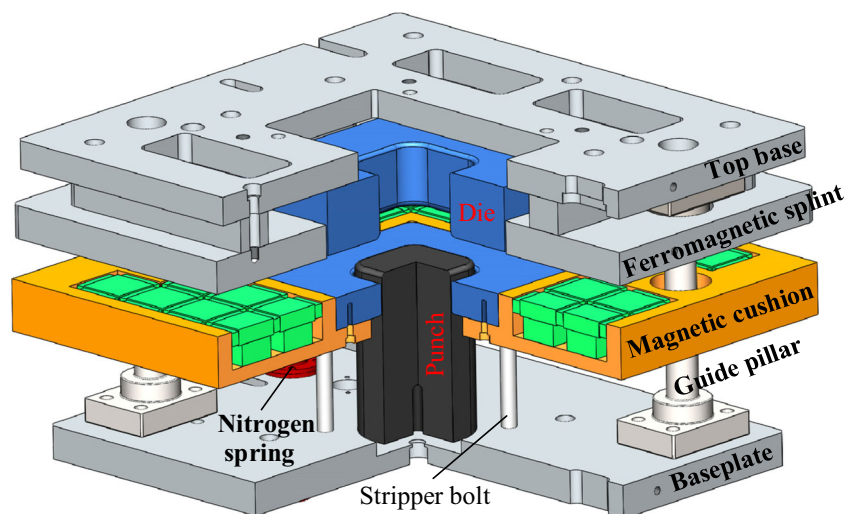
Fig. 1 can be divided into three subdivisions: upper assembly, magnetic cushion and baseplate. The upper assembly is mainly composed of the top base, the ferromagnetic splint, and the die between them. The baseplate is fixed on the base platform. The magnetic force can be generated in the magnetic cushion, which contains a magnetized zone and a blank holder zone. The weight of the cushion is balanced by the nitrogen springs, which hardly provides any BHF. The magnetic force generated by permanent magnets only exists in the magnetized zone and can be applied on sheet metal through the blank holder in the form of BHF. Since the instantaneous currents are only needed at the moment of applying or removing BHF, there is no power loss for maintaining BHF during the deep drawing process, and it will not cause the loss of excitation accident even when the power is off.

As shown in Fig. 1, the deep drawing process with ECBH can be like this:

Deep drawing stage: When the process starts, the upper assembly moves down under the drive of the press slide. An instantaneous DC pulse current is imposed to the coils once the upper assembly is about to contact the magnetic cushion. The upper assembly can be firmly attracted to the cushion under the action of the magnetic attractive force generated by the closed magnetic circuit between them, which is called ON state. Then, the flange of sheet metal can be tightly pressed on the blank holder by the die. The magnitude of BHF can be adjusted by the instantaneous current intensity. As the cushion moves down together with the upper assembly, the sheet metal contacts the punch and is gradually drawn.

Return stroke: the press slide begins to return upwards after the drawing process is completed. Since the magnetic force still exists between the upper assembly and the cushion at this time, the magnetic cushion and the upper assembly return synchronously. During this period, the drawn part can be gradually separated from the punch under the action of the cushion in upward motion. Before the cushion reaches the

Fig. 1 Schematic diagram of equipment with ECBH



original position, a reverse DC pulse current is imposed into the coils to change the magnetic circuit of the magnetic field. That is, the magnetic cushion is turned from ON state to OFF state, and there will be almost no magnetic field and the resulting attractive force between the ferromagnetic splint and the magnetic cushion. Then, the magnetic cushion stops at its original position under the combined effect of nitrogen spring and stripper bolt. As the upper assembly continues to move upward with the press slide, the drawn part is thoroughly separated from the punch.

3 Magnetic element and magnetic circuits

3.1 Magnetic circuit of magnetic element

The magnetic element (ME) is the basic structural unit that generates the magnetic field in the magnetized zone of the magnetic cushion. The basic magnetic circuits of the ON state and OFF state can be obtained and exchanged utilizing a pair of MEs. In fact, the two pairs of MEs are the main structure of magnetic cushion, as exhibited in Fig. 2. There are four magnetizers at the top level, each surrounded by four fixed magnets (FMs). There is a reversible magnet (RM) under each FM, and is wrapped on the outside by the coils.

Also, it is necessary to introduce the properties of the selected materials for each component, which is the basis for understanding the working principle of the magnetic circuit. The RM is made of soft magnetic material which has a thin loop area of magnetic hysteresis that the direction of the magnetic field can be permanently adjusted through a small external magnetic field. Conversely, the hard magnetic material with an obese loop area is used as FM, because its polarity is constant and is hardly changed. The magnetizer made of pure iron is used to pass the magnetic field lines. It should be noted that both FM and RM are permanent magnets rather than electromagnets.

As shown in Fig. 3, a micro magnetic cushion is exemplified to explain the working principle of the magnetic circuits.

There is only one pair of MEs in the micro cushion, which is sealed in the shell by epoxy resins.

Fig. 3a shows the micro magnetic cushion in OFF state that the adjacent magnetic poles of FMs and RMs are different. For example, the magnetic pole of the FM closest to the S-pole side of RM is the N-pole side, and vice versa. In this state and according to the law of the magnetic field, the magnetic circuits can only be closed inside the cushion. Therefore, the ferromagnetic splint is free because of the absence of magnetic field lines outside the cushion.

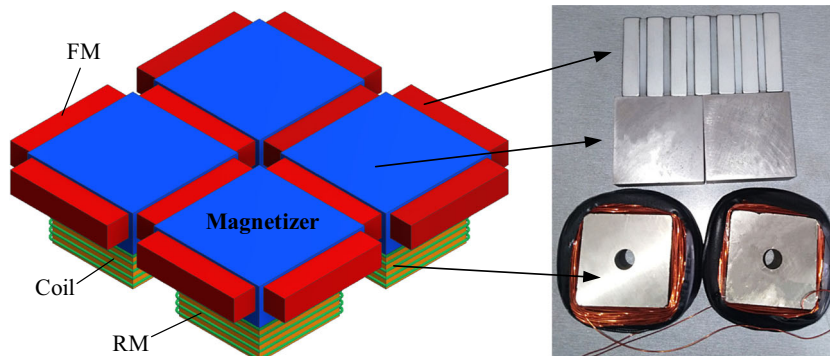
When the coil winding is energized by an instantaneous current, a temporary electromagnetic field is generated. As shown in Fig. 3b, the magnetic poles of RMs can be reversed by this temporary electromagnetic field, and will remain stable after the external electromagnetic field is removed. If the magnetic field lines from the N-pole sides of RMs and FMs want to reach the nearest S-pole sides, they will pass through the ferromagnetic splint. This means that the ferromagnetic splint can be attracted to the magnetic cushion through the magnetic attractive force between them, which is called the ON state. Moreover, only a reverse current pulse is required to switch back to the OFF state again.

Figure 4 shows the magnetic hysteresis switching of RM from OFF state to ON state. A temporary external electromagnetic field is generated by applying a single DC pulse current through the coil windings. This external magnetic field is strong enough to modify the magnetic pole direction of RM because of the nature of the RM.

It should be noted that after the magnetic cushion is manufactured, all internal parts are fixed and can no longer be replaced. The magnitude of the magnetic force and resulting BHF can be adjusted by changing the intensity of the instantaneous external input current pulse. In this way, only the magnetic pole directions of the RMs can be changed, and the PMs remain unchanged.

As shown in Fig. 4a and corresponding Fig. 3a, during the OFF state, the working point of RM is at one of the vertices of the curve. As shown in Fig. 4b, the working point can be moved along the magnetic hysteresis curve towards the lower vertex through the external electromagnetic field, and stop at a

Fig. 2 Schematic diagram of two pairs of MEs



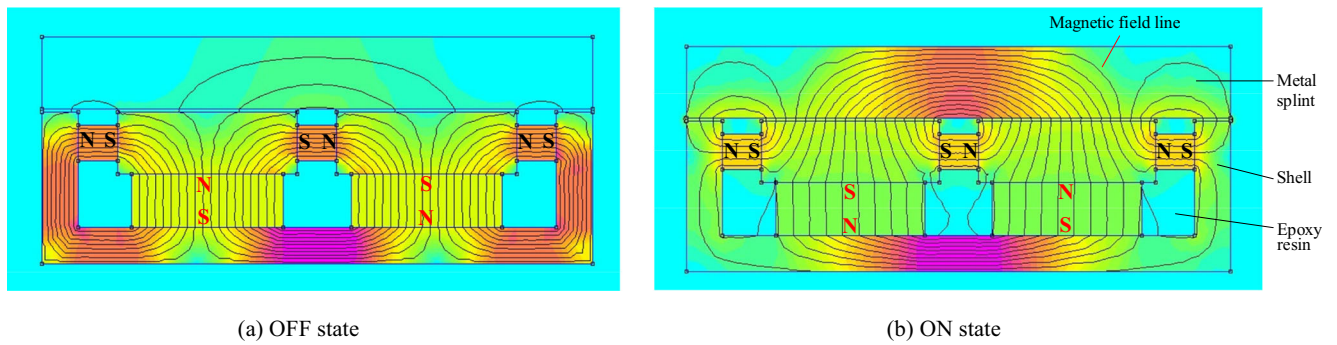


Fig. 3 Micro magnetic cushion in ON and OFF states. **a** OFF state, **b** ON state

certain position according to the strength of the external magnetic field. The ON state can be achieved when the working point arrives at the lower vertex if the external magnetic field is strong enough, as shown in Fig. 4c and corresponding Fig. 3b. As shown in Fig. 4d, the working point can move back to the top vertices along another line of the curve when the reverse current is applied. For switching the states of cushion, t , the energizing time of the DC pulse current (intensity is C_a and C_b) is equal to 20 ms, both ON and OFF states. No current is required during other periods of the deep drawing process cycle T .

3.2 Verification of magnetic circuit effectiveness

For isotropic media and considering the normal flux density, the force of the magnetostatic field on the magnetic target can be calculated by the Maxwell stress tensor methods:

$$F_m = \iiint_V (\nabla \times M) B dV \tag{1}$$

where M is the magnetization intensity of the magnetic target, $M = (\mu_r - 1)B/2\mu_0\mu_r$, $\nabla \times$ is the curl operator, B is the magnetic flux density, μ_0 is the magnetic permeability of the vacuum and μ_r is the relative permeability of the magnetic medium. Substituting the expansion of M into Eq. (1), Eq. (2) can be obtained as:

$$F_m = \frac{\mu_r - 1}{2\mu_0\mu_r} \iiint_V \nabla \times B^2 dV = \frac{\mu_r - 1}{2\mu_0\mu_r} \iint_S B^2 dS \tag{2}$$

We generally assume that the magnetic field distributed is uniform, and μ_r can be eliminated from Eq. (2) because of $\mu_r \gg 1$. So,

$$F_m = \frac{B^2 S}{2\mu_0} = \frac{\sum B_n^2 S_n}{2\mu_0} \tag{3}$$

where B_n and S_n are the magnetic flux density and the area of each EM, respectively.

Therefore, the factors that affect the magnetic force of the magnetic cushion are the materials of FM and RM, the dimension and shape of each component of the cushion. More importantly, the realization of OFF state also depends on the reasonableness of the above parameters. Furthermore, the setting of coil winding depending on these parameters determines the value of C_a , and further affect the temperature rise of the cushion during continuous deep drawing operations. Finally, the materials and dimensions selected are listed in Table 1.

To verify the effectiveness of the designed EM and its magnetic circuit, the ANSYS software was used for finite element analysis (FEA). A 3-D micro magnetic cushion model including four EMs was established and meshed by Solid98

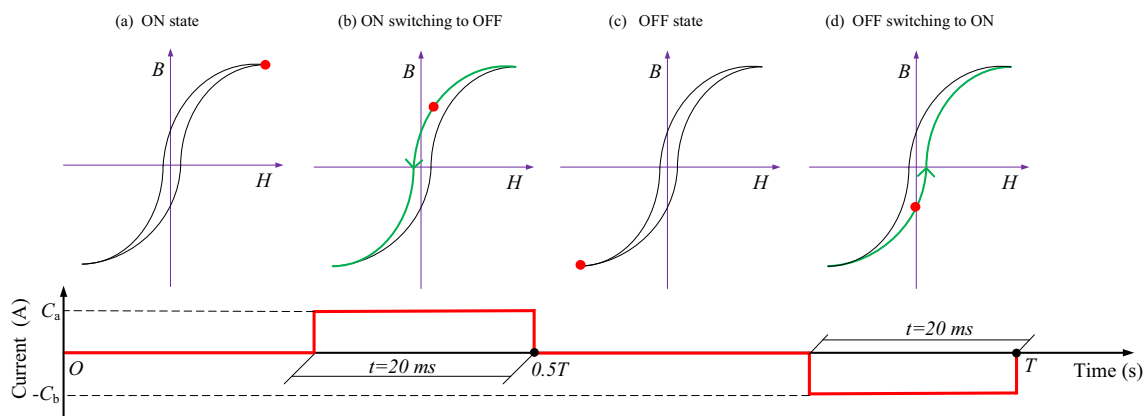


Fig. 4 Magnetic hysteresis of RM in different states

Table 1 Materials and dimensions of EM

Components	Materials	Properties
RM	AlNiCo	38 × 38 × 15 mm
FM	NdFeB	44 × 10 × 10 mm
Magnetizer	Iron	50 × 50 × 17 mm
Coil winding	Copper wire	300 turns each EM

element. The reduced scalar potential strategy [20] was adopted in the FEA to solve Laplace’s equation followed by the magnetic scalar potential. The results of magnetic flux density are shown in Fig. 5.

Figure 5a presents the simulated result of the micro cushion in the ON state, in which most of the magnetic field lines pass the ferromagnetic splint. The maximum resulting magnetic attractive force between the cushion and ferromagnetic splint is 15833 N. As shown in Fig. 5b, in the OFF state, almost all the magnetic field lines are only transmitted internally and do not leave the cushion. As such, the corresponding magnetic force is extremely small, only about 7 N. These results indicated that the designed EM can realize the two predetermined magnetic circuits.

For further verification, the magnetic attractive force of the micro magnetic cushion including four EMs was tested using the tensile machine. The test result presented in Fig. 6 shows that the maximum magnetic force is more than 16,000 N, which can meet the requirement of blank holding.

3.3 Thermal analysis and test of micro magnetic cushion

Usually, a deep drawing cycle in the industry may take a few seconds. There is one ON state and two OFF states (beginning and ending) in each stamping process. The states of magnetic cushion need to be switched twice in a cycle, that is, two short-term currents are required. To avoid the situation where BHF is limited by temperature rise as in electromagnetic technique, it is necessary to investigate the temperature variation of the magnetic cushion to meet the requirement of continuous deep

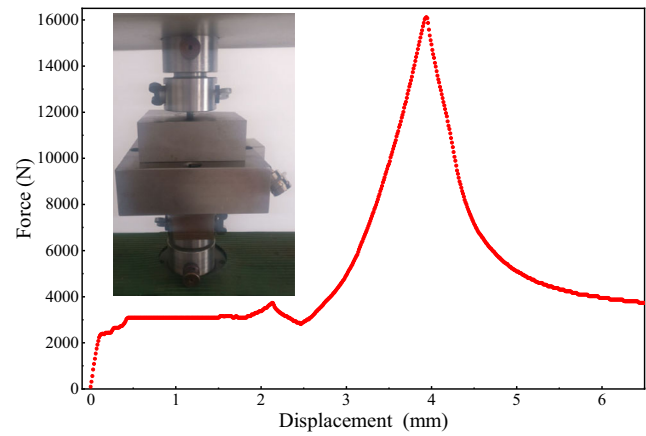


Fig. 6 Tensile test for measuring magnetic force

drawing operation. The transient thermal analysis using ANSYS software was adopted. The FEA grid model and test system of the micro magnetic cushion including two EMs are shown in Fig. 6. We choose $T = 4$ s as the analysis condition and assuming the deep drawing operation lasts for about 3 h. To make the analysis and test more conservative, the maximum $C_a = 15$ A and $C_b = 8$ A were energized. A load cycle T (including one normal energization and one reverse energization) was repeated with the help of looping statements for 3 h.

Figure 7 shows the simulated temperature distribution of the micro magnetic cushion after nearly 180 min of operation. The maximum temperature of 41.5 °C occurs in the region between the two RMs. Fig. 8 shows that the corresponding maximum temperatures varied with time derived from the test measurement and the transient thermal analysis, respectively. The experimental results show that the temperature first goes through a rapid growth process in a very short period and then slows down. After 180 min of continuous operation, the maximum temperature of the experimental micro cushion is about 42.8 °C. Back to the thermal simulation, in the initial stage of transient heat transfer, the rapid temperature rise is far less than the experimental results. This is because the temperature sensor used in the test is embedded in the coil windings, whereas in the FEA the heat flux is applied directly to the side faces of the RMs. As time increases, the thermal field gradually reaches equilibrium, and the temperature difference

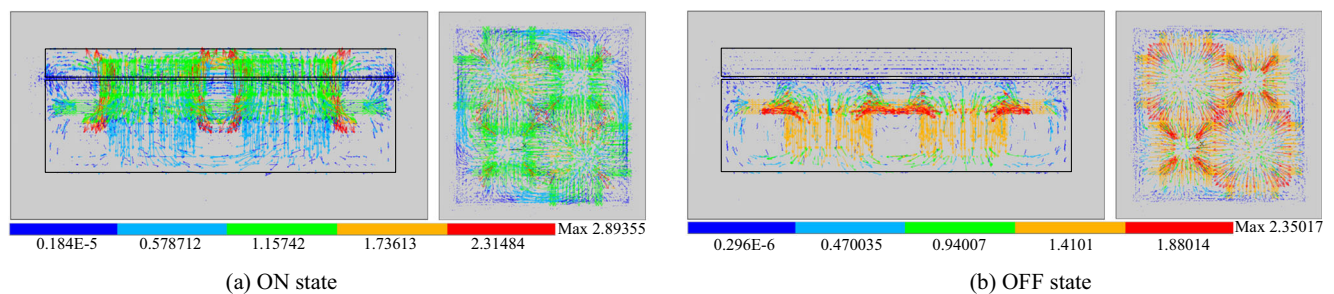
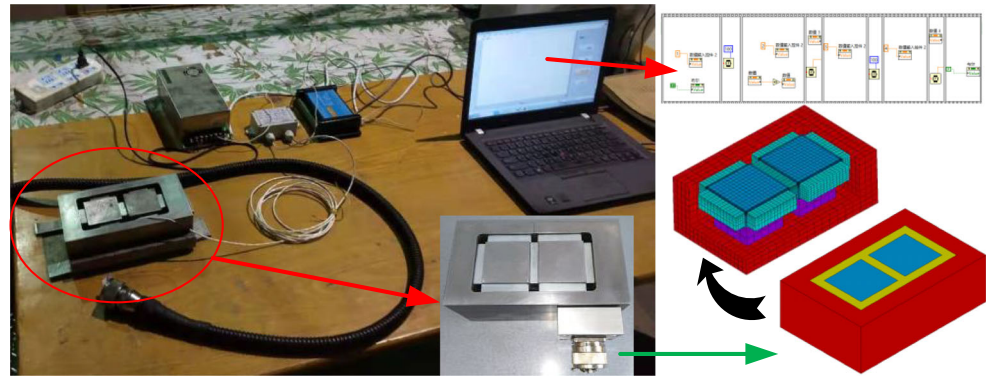


Fig. 5 Magnetic flux density of micro magnetic cushion including four EMs. **a** ON state, **b** OFF state

Fig. 7 System of temperature measuring and simulation



between the two parts will be eliminated. Therefore, at the cutoff time, the simulated temperature is close to the tested temperature.

4 ECBH technique

4.1 Magnetic cushion

Figure 9a shows the magnetic cushion with the conventional single blank holder, which is made of a single piece of steel. For the sake of avoiding magnetizing the sheet metal, the MEs can only be arranged in the magnetized zone but not in the blank holder zone. There is a total of 46 MEs, which are symmetrically arranged in the magnetized zone with blank holder as the center. Due to the need to provide corresponding BHF for sheet metals with different sizes, the magnetic force provided by the magnetic cushion should be adjustable. For this reason, the magnetic flux density generated by the designed magnetic cushion is divided into 16 levels which can provide 16 different magnetic flux densities and BHF levels. The levels of the magnetic flux density and BHF can be controlled by the intensity of energizing instantaneous currents.

Figure 9b exhibits the magnetic cushion with the combined blank holder, in which only the blank holder is replaced and the others are exactly the same as those shown in Fig. 9a. The combined blank holder is designed to be of two layers: the base layer made of polyurethane rubber with high strength and good elasticity, and the top blank holder divided into several segments along circumferential and radial directions respectively. Although the permanent magnet system provided is the same for both, the structure of the blank holder is different. Under the condition of using the same magnetic cushion level, the total BHF produced by the two structures is the same, but the distribution is different. In fact, the increments of flange thicknesses in the outside regions are always greater than those in the inside regions during deep drawing. So, when the blank holder is a single piece of steel plate, most of the BHF is applied on the flange periphery due to the increased thickness. That is, the inner area will obtain a small BHF so that the wrinkling cannot be well suppressed. However, when using the new blank holder technique, even if the thickness of the outer flange sheet is increased, since the inner blank holder piece is independent of the outer blank holder piece, the sufficient BHF can be independently applied by the inner blank holder piece without being affected by the outer blank holder

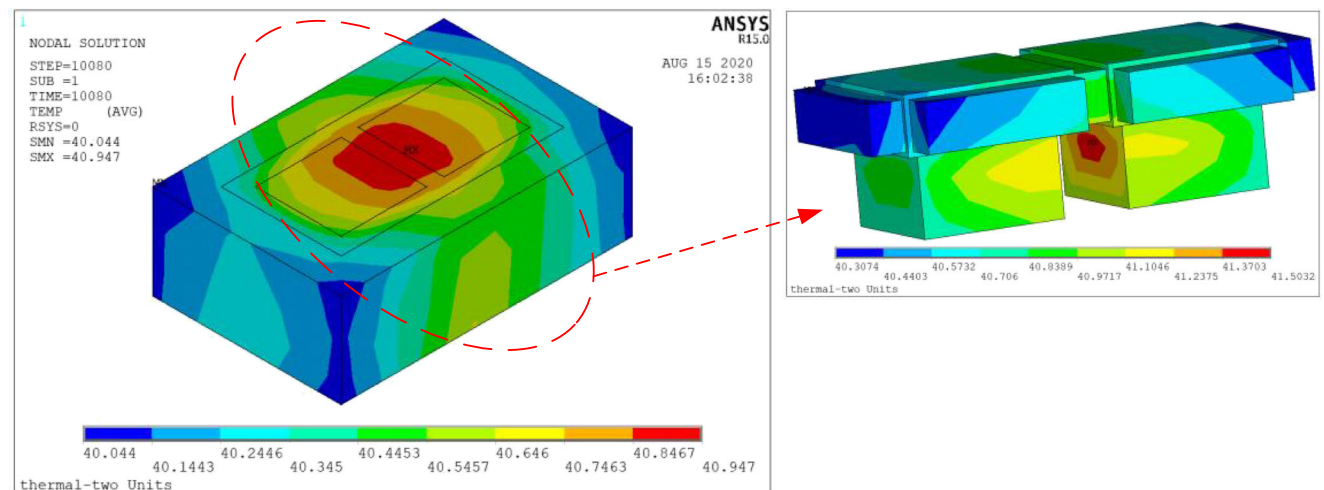


Fig. 8 Change in maximum temperature of ME

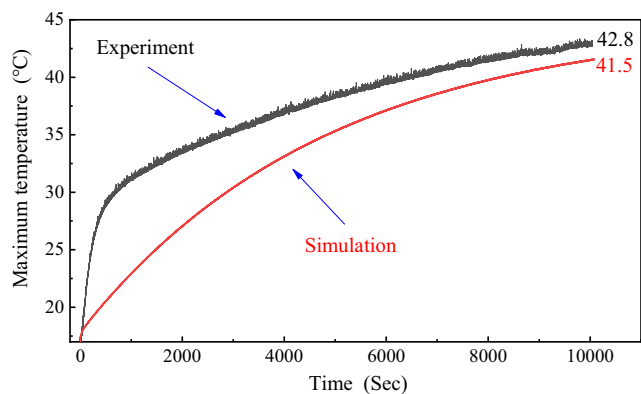


Fig. 9 Schematic diagram of magnetic cushion. a Single blank holder, b combined blank holder

piece. This arrangement ensures that each segment can work effectively and independently.

4.2 Principle and superiority of combined blank holder technique

Since the MEs cannot be arranged in the blank holder zone but only in the magnetized zone, it can be expected that the BHF will concentrate more on the flange edge. That is, the blank holder pressure (BHP) on the periphery of the flange will be much greater than on the inside. So, the new combined blank holder technique was proposed, in which the radial segmental technique combined with the circumferential segmental blank holder.

The role of the new blank holder technique is to limit the excessive circumferential stress in the blank plane to cause wrinkling. So, the BHF in each circumferential area can be independently applied on the blank holder, and then transferred to the flange of the drawn part. Since the new blank holder technique can optimize the radial and circumferential distribution of BHF at the same time, it can better improve the forming effect of the blank compared with the traditional blank holder method.

4.2.1 Radial segmental technique in the rounded corner zones

The traditional theory holds that the wrinkling model [21] of axisymmetric parts in deep drawing can be mathematically expressed as Eq. (4).

$$y = y_0 \left(\frac{1}{2} - \frac{1}{2} \cos \frac{2\pi\phi}{\phi_0} \right) \left(\frac{R-r}{R_t-r} \right)^{0.5} \tag{4}$$

where y is the displacement of the wrinkle in a certain radial coordinate coordinates R , r and R_t are the radii of the die and flange edge, respectively, y_0 is the maximum displacement of all wrinkles (MDW), ϕ_0 is the whole polar angle of a single wrinkle wave along the circumferential direction, and ϕ is the polar angle of the specified arc in the single wrinkle wave.

According to this theory, the amplitudes of the wrinkle displacement on the flange edge are larger than that of the inside regions. So, the critical BHP for suppressing wrinkling can be written as Eq. (5).

$$p = \frac{(\sigma_s + \sigma_b)R \left[\frac{2(R-r-r_d)}{\delta} - 8 \right]}{90\pi \left[R^2 - (r-r_d)^2 \right]} \tag{5}$$

where p is the critical BHP for suppressing wrinkling in a certain radial position, r_d is the radius of die arc, σ_s and σ_b are the yield strength and the tensile strength, respectively, and δ is the thickness of the sheet metal.

In this case, most of the BHP can only be forced on the flange periphery due to the greater thickness. Theoretically, wrinkling can be well suppressed in the flange edge, and the wrinkling model can be described as the curve shown in Fig. 10a. Under the action of sufficient BHF, the wrinkle amplitude at the flange edge is effectively reduced. So, the slope of the curve changes at a certain point, R_c , and Q_c and Q_0 are the BHF applied on point R_c and R_t respectively. In this case, the mathematical model of Eq. (4) is imperfect, and it should be described as Eq. (6) for matching Fig. 10a. According to this equation, MDW will occur at the flange edge.

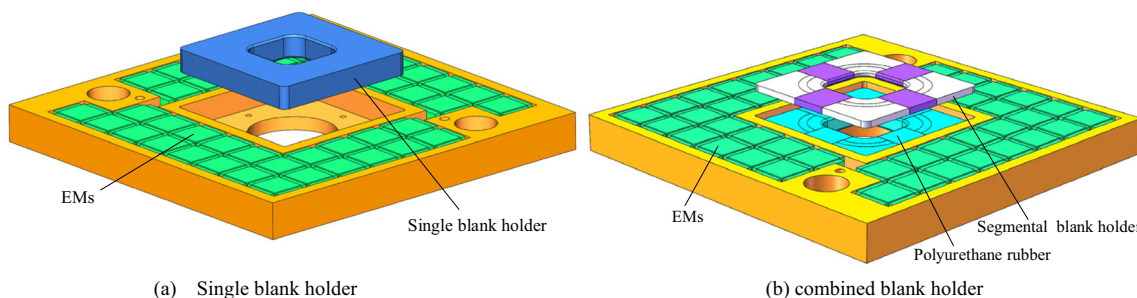


Fig. 10 Radial wrinkling model using different blank holders

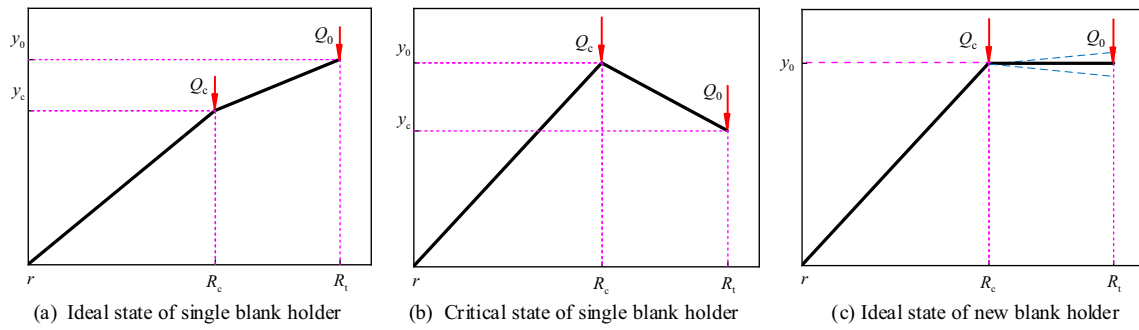


Fig. 11 The magnetic flux density distribution in ON state. **a** Surface plot of magnetic cushion. **b** Surface plot of ferromagnetic splint

$$y = \begin{cases} \frac{y_0(R-r) \left[1 - \cos\left(\frac{2\pi\phi}{\phi_0}\right) \right]}{2(R_c-r)} & R \leq R_c \\ \frac{\left[\frac{(R-R_c)(y_0-y_c)}{(R_r-R_c)} + y_0 \right] \left[1 - \cos\left(\frac{2\pi\phi}{\phi_0}\right) \right]}{2} & R > R_c \end{cases} \quad (6)$$

$$y = \begin{cases} \frac{y_0(R-r) \left[1 - \cos\left(\frac{2\pi\phi}{\phi_0}\right) \right]}{2(R_c-r)} & R \leq R_c \\ \frac{y_0}{2} \left[1 - \cos\left(\frac{2\pi\phi}{\phi_0}\right) \right] & R > R_c \end{cases} \quad (7)$$

However, in practice, most of the BHF are mainly acted on a narrow region of the flange periphery since the thickness of the flange edge will significantly increase during deep drawing. Therefore, at the critical state of wrinkling, when wrinkles are completely suppressed by a large enough Q_0 , the wrinkles on the inner flange metal may be the largest because of the lack of suppression, as shown in Fig. 10b.

This deficiency can be overcome by the blank holder divided into several pieces radially, by which BHF can be reasonably distributed and MDW can be effectively reduced. Ideally, the MDW in the region between point R_c and point R_t can be the same if the ratio of Q_c to Q_0 is proper, because BHF applied by each segment can be forced independently to different radial flange regions. At this point, the curve and its mathematical expression can be improved to Fig. 10c and Eq. (7), respectively.

4.2.2 Theoretical validation for radial segmental blank holder in rounded corner zones

There are two kinds of deformation energies during the wrinkling of flange metal: the energies required to bend the metal, U_1 , and the energies released by circumferential stress, U_2 . There is another energy used to balance those two deformation energies during deep drawing for suppressing wrinkling, that is, pressing energy applied by the external force blank holder, U_3 . And according to the law of energy conservation [22, 23], those three energies must be balanced at the critical state of flange metal wrinkling and instability.

$$U_3 = U_2 - U_1 \quad (8)$$

Based on the energy method used in flange wrinkling [24], U_1 required for a single wave can be written as Eq. (9).

Fig. 12 The magnetic flux density distribution in OFF state. **(a)** Surface plot of magnetic cushion. **(b)** Surface plot of ferromagnetic splint

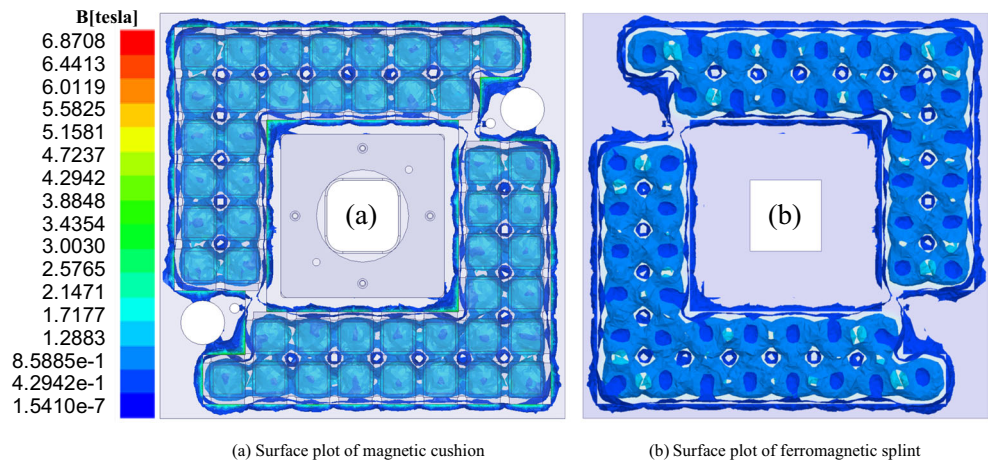
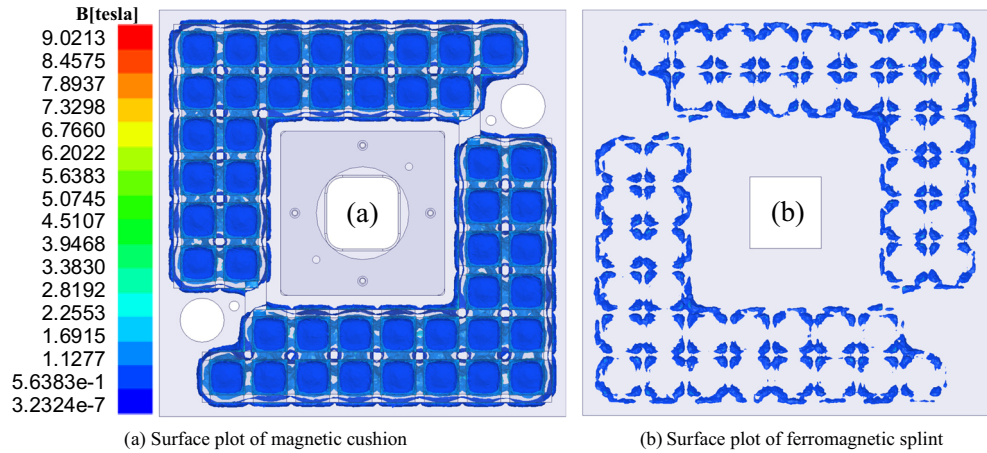


Fig. 13 The size parameters of segmental blank holder



$$U_1 = \frac{kn\delta^3\pi^4}{12\phi_0^3} \left(\ln\frac{R_0}{R_t}\right)^{n-1} \int_{r_t}^{R_t} \frac{[f(R)]^2}{R^3} dR \tag{9}$$

where k is the hardening coefficient, n is strain hardening index, and $f(R)$ is divided into two parts, as shown in Eq. (10).

$$f(R) = \begin{cases} \frac{R-r}{R_c-r} y_0 & R \leq R_c \\ \left[\frac{(1-\lambda)(R-R_c)}{R_t-R_c} + 1 \right] y_0 & R > R_c \end{cases} \tag{10}$$

where $\lambda = y_c/y_0$.

Similarly, U_2 caused by circumferential stress can be calculated by Eq. (11).

$$U_2 = -\frac{k\delta\pi^2}{4n\phi_0} \left(\ln\frac{R_0}{R_t}\right)^{n-1} \int_{r_t}^{R_t} \frac{(1-n)R_t^n - R^n}{R^{n+1}} [f(R)]^2 dR \tag{11}$$

Since $f(R)$ is divided into two parts based on point R_c , so is U_3 .

For the wrinkling model using the single blank holder shown in Fig. 10b, substituting Eq. (9) and Eq. (11) into Eq. (8), we will have:

$$U_3 = \begin{cases} -\frac{k\delta\pi^2}{4n\phi_0} \frac{y_0^2}{(R_c-r)^2} \ln\left(\frac{R_0}{R_t}\right)^{n-1} \int_{r_t}^{R_t} \frac{(R-r)^2 [(1-n)R_t^n - R^n]}{R^{n+1}} dR - \frac{kn\delta^3\pi^4}{12\phi_0^3} \frac{y_0^2}{(R_c-r)^2} \ln\left(\frac{R_0}{R_t}\right)^{n-1} \int_{r_t}^{R_t} \frac{(R-r)^2}{R^3} dR & R \leq R_c \\ -\frac{k\delta\pi^2}{4n\phi_0} y_0^2 \ln\left(\frac{R_0}{R_t}\right)^{n-1} \int_{r_t}^{R_t} \frac{\left[\frac{(R-R_c)(1-\lambda)}{R_t-R_c} + \lambda\right]^2 [(1-n)R_t^n - R^n]}{R^{n+1}} dR - \frac{nk\delta^3\pi^4}{12\phi_0^3} y_0^2 \ln\left(\frac{R_0}{R_t}\right)^{n-1} \int_{r_t}^{R_t} \frac{\left[\frac{(R-R_c)(1-\lambda)}{R_t-R_c} + \lambda\right]^2}{R^3} dR & R > R_c \end{cases} \tag{12}$$

For the wrinkling model using the segmental blank holder shown in Fig. 10c, Eq. (12) for this case becomes:

$$U'_3 = \begin{cases} -\frac{k\delta\pi^2}{4n\phi_0} \frac{y_0^2}{(R_c-r)^2} \ln\left(\frac{R_0}{R_t}\right)^{n-1} \int_{r_t}^{R_t} \frac{(R-r)^2 [(1-n)R_t^n - R^n]}{R^{n+1}} dR - \frac{kn\delta^3\pi^4}{12\phi_0^3} \frac{y_0^2}{(R_c-r)^2} \ln\left(\frac{R_0}{R_t}\right)^{n-1} \int_{r_t}^{R_t} \frac{(R-r)^2}{R^3} dR & R \leq R_c \\ -\frac{k\delta\pi^2 y_0^2}{4n\phi_0} \ln\left(\frac{R_0}{R_t}\right)^{n-1} \int_{r_t}^{R_t} \frac{[(1-n)R_t^n - R^n]}{R^{n+1}} dR - \frac{nk\delta^3\pi^4 y_0^2}{12\phi_0^3} \ln\left(\frac{R_0}{R_t}\right)^{n-1} \int_{r_t}^{R_t} \frac{1}{R^3} dR & R > R_c \end{cases} \tag{13}$$

So, the energy required by the two blank holder methods under the same MDW condition is different. Based on Eq. (13) and Eq. (12), we have the following:

$$U'_3 - U_3 = \frac{k\delta\pi^2 y_0^2 (1-\lambda)^2}{4n\phi_0 \lambda (R_t - R_c)^2} \ln\left(\frac{R_0}{R_t}\right)^{n-1} \left[\int_{R_c}^{R_t} \frac{(R-R_c)^2 [(1-n)R_t^n - R^n]}{R^{n+1}} dR + \frac{n^2\delta^3\pi^2}{3\phi_0^2} \int_{R_c}^{R_t} \frac{(R-R_c)^2}{R^3} dR \right] \tag{14}$$

Predictably, Eq. (14) must be less than zero since λ and n are less than 1 (for 08Al material, $n = 0.23$). That is, the energy consumed by the radial segmental blank holder is lower than the single blank holder for suppressing the same MDW, and the required BHF is also smaller. So, because the deformed metal in the rounded corner zones can be effectively suppressed by a smaller

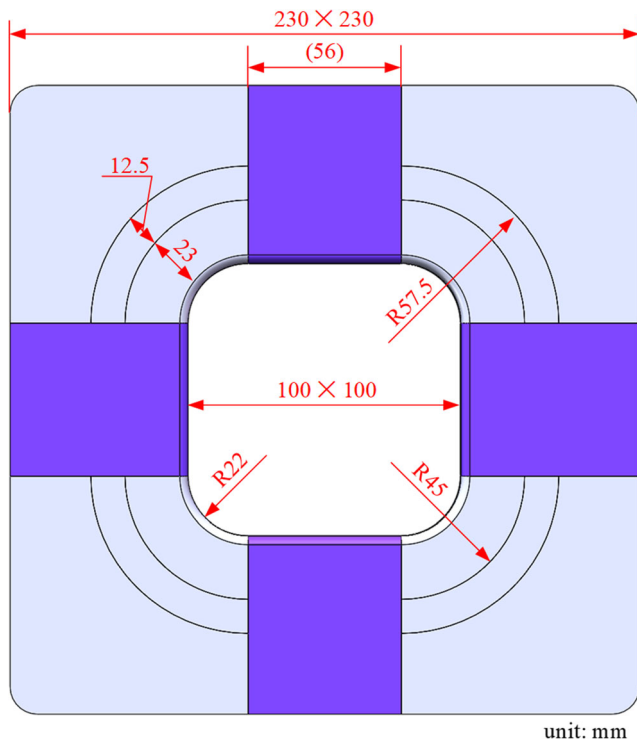


Fig. 14 Distribution of BHP. **a** Single blank holder. **b** Segmental blank holder

BHF, the holding effect will be improved using the radial segmental blank holder.

4.2.3 Circumferential segmented blank holder

Similar to the rounded corner zones, it should also be beneficial to segment radially in the straight flange zones. However, a single blank holder is used in the straight flange zones, because the thicknesses of metal are more uniform in these parts.

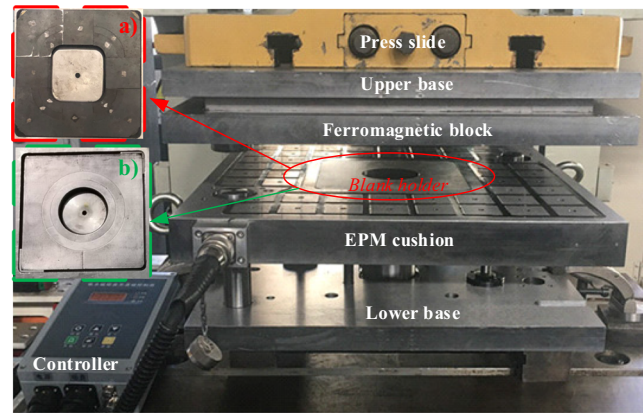


Fig. 16 Photograph of upright experimental setup for, **(a)** Square box, **(b)** Axisymmetric cup

In other words, the blank holder is segmented along the circumferential direction, and the rounded corner zones are further segmented in the radial direction, as shown in Fig. 9b. In this way, the two kinds of circumferential zones can be held independently and effectively. So, BHF can be reasonably distributed both in the circumferential and radial directions.

4.3 Magnetic field analysis of magnetic cushion

To evaluate the effectiveness of the designed magnetic cushion, the magnetic field analysis was carried out using the MAXWELL software application. Fig. 11a shows the magnetic flux density distribution of magnetic cushion when the maximum level was selected, in which the magnetic flux density and the generated magnetic force reached the highest limit. It can be observed that almost all the magnetic fields exist in the magnetized zone, but there is nearly no magnetic flux density in the blank holder zone. Fig. 11b is the magnetic flux density distribution in the ferromagnetic splint, in which

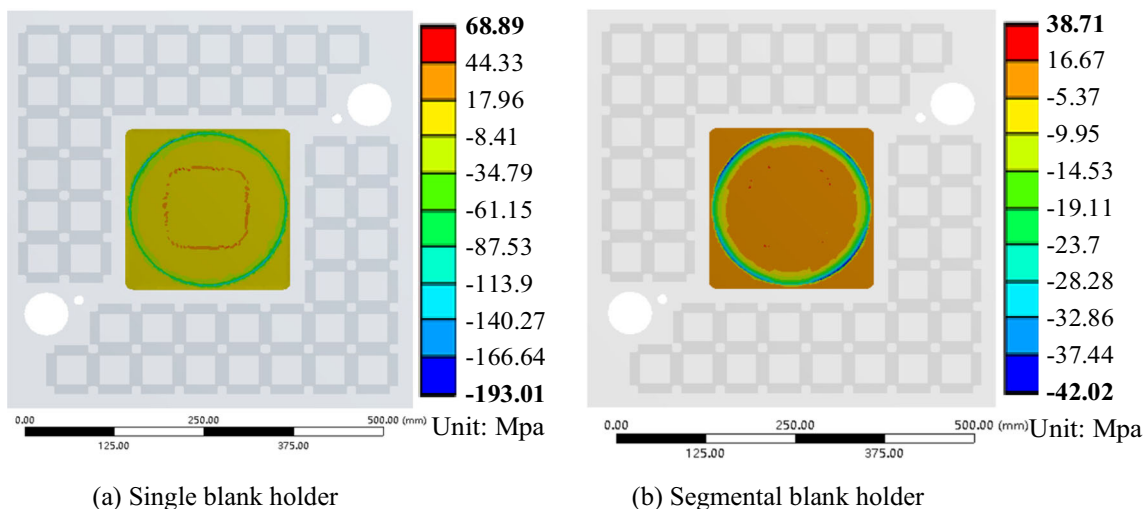
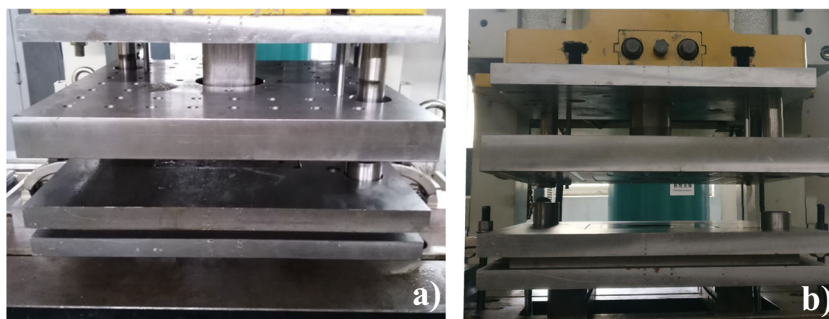


Fig. 15 Photograph of inverted experimental setup for, **(a)** Square box, **(b)** Axisymmetric cup

Fig. 17 Photograph of square boxes, (a) Single blank holder, (b) combined blank holder



magnetic flux is distributed in the region above the magnetized zone. As shown in Fig. 12, the magnetic cushion is adjusted to the OFF state by energizing a reverse instantaneous current. The magnetic flux density is close to zero on the surface of the magnetic cushion and in the ferromagnetic splint. Due to the high concentration of magnetic field lines closed inside the magnetic cushion, the maximum magnetic flux density inside the magnetic cushion is greater than that in the ON state.

Results from magnetic field analysis show that magnetic cushion can be successfully converted between ON state and OFF state without affecting the blank holder zone.

4.4 BHP distribution on the sheet metal

To evaluate the effectiveness of the combined blank holder, the stress analyses were carried out by WORKBENCH applications, in which the FE model including cushion, ferromagnetic splint, and the sheet metal between them was created. The magnetic force calculated by magnetic field analysis was applied on the magnetized zone along the vertical direction.

For the designed blank holder method, the BHP applied by each segmental blank holder can be different and independent. But in fact, the key factors for optimizing the force applied by each segment are their parameters, such as the boundary diameter, the radius of chamfer, the length of the straight side, etc. Based on a large amount of orthogonal analysis, the final optimized segmental blank holder is shown in Fig. 13. Once a parameter is changed, it will affect the distribution of BHP.

The results of stress analysis based on this set of parameters are shown in Fig. 14. Fig. 14b presents the distribution of contact pressure (that is, BHP) on the sheet metal. For comparison, a similar analysis was carried using the single blank holder, the result is shown in Fig. 14a. Almost all BHPs are concentrated in small peripheral areas under the action of the single blank holder. On the bright side, BHP shown in Fig. 13b is distributed over a very wide radial area using the combined blank holder.

What's more, as the flange edge becomes thicker in the deep drawing, BHP will be more concentrated on the flange peripheral. Since each block of the blank holder can be moved independently, the scope of BHP applied by the combined blank holder technique will be wider. It can be predicted that the forming effect can be improved using the new blank holder technique.

5 Forming experiment for ECBH system

Fig. 15 presents the key components of equipment for validating the effectiveness of the proposed blank holder technique. The current controller can adjust the current intensity according to instruction. Fig. 15a shows the combined blank holder for drawing square box, and Fig. 15b shows the segmental blank holder for the axisymmetric part which is equivalent to the rounded corner zone of square box theoretical analyzed in Section 4.2. Actually, the designed cushion also can be used for upright drawing setup, as exhibited in Fig. 16.

Fig. 18 Photograph of axisymmetric drawn cups, (a) Single blank holder, (b) Segmental blank holder

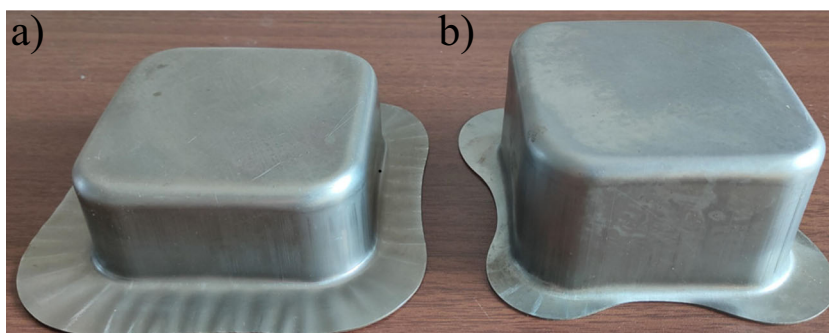
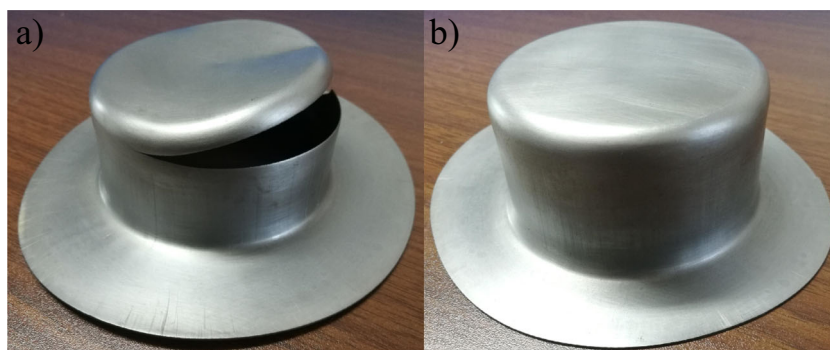


Fig. 19 Experimental setup for radial segmental technique



For square box deep drawing, the 08Al sheets with thickness of 1 mm and diameter of 200 mm were used when a level 7 of magnetic flux density was selected in the experiment. As presented in Fig. 17a, there are serious wrinkles on the rounded corner zones of the drawn part using the single blank holder when the drawing height is about 38 mm. As shown in Fig. 17b where the drawing height is about 50 mm, wrinkling was completely suppressed for the same sheet metal using the new blank holder.

This happened mainly because BHF was concentrated on the peripheral regions of the flange using the single blank holder. In contrast, since every piece of the blank holder can force BHF freely both in radial and circumferential directions, the distribution of BHP is more reasonable using the segmental blank holder. Therefore, there are neither wrinkles nor cracks on the drawing part shown in Fig. 16b.

Differently, a relatively larger BHF was applied on the axisymmetric cups to verify the ability to suppress cracks. The 08Al sheets with diameter of 190 mm were selected. As expressed in Fig. 18, the drawn cups with height of 45 mm were obtained when level 6 was selected. Since most of BHF is concentrated on the flange edge and seriously restricts the reasonable material flow, there is a large crack at the punch corner of the drawn cup using the single blank holder, as shown in Fig. 18a. At the same drawing height and using the new blank holder method, there are neither cracks nor wrinkles on the drawn cup, as shown in Fig. 18b.

In summary, because the distribution of BHP is more reasonable, using the ECBH can both effectively improve the deformability of the axisymmetric drawn cup and square box.

6 Verification of universality of radial segmental technique

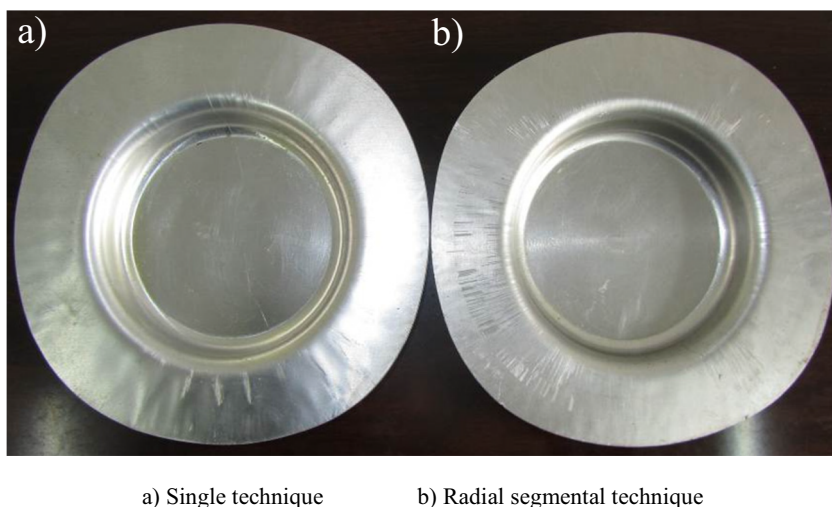
In order to verify the universality and versatility of the application of the radial segmental technique, a deep drawing setup using segmental blank holder is designed, as shown in Fig. 19. In this experimental setup, the blank holder is divided radially in the form of a double ring, in which the effect of magnetic field is removed and the distribution of BHF is considered only.

Fig. 20 shows the drawn parts with 33 mm height of AA3003 material when the value of BHF was 12 kN. As shown in Fig. 20a, wrinkles at the periphery were well suppressed, but there were obvious wrinkles far from the edge. This is because the BHF applied on the flange periphery was sufficient to suppress wrinkles, and the internal zones cannot be effectively held under insufficient BHF. However, as shown in Fig. 20b, the wrinkles were substantially suppressed on the whole flange using the double ring blank holder, in which the BHF distribution was more reasonable to suppress wrinkles both on the flange periphery and internal zones.



Fig. 20 Drawn cups of AA3003 sheet. **a** Single technique. **b** Radial segmental technique

Fig. 21 The BHP initial distribution along the radial direction



To study the influence of boundary diameter W between the inner ring and the outer ring on the BHP distribution, the stress analysis was carried out by ANSYS software. The simulated result is shown in Fig. 21, BHP applied on the sheet metal basically increases as the radial coordinate increases. The boundary diameter W has a greater impact on the distribution of BHP. The smaller W , the more uniform distribution of BHP in the radial direction. But it should be noted that too uniform distribution is not beneficial, because the flange periphery requires a larger BHP. Therefore, when BHP on the peripheral areas can suppress wrinkles, a smaller W can suppress the internal particles more effectively.

Through these analyses and experiments, it can be further proved that the radially segmented blank holder can apply different BHP in different radial regions.

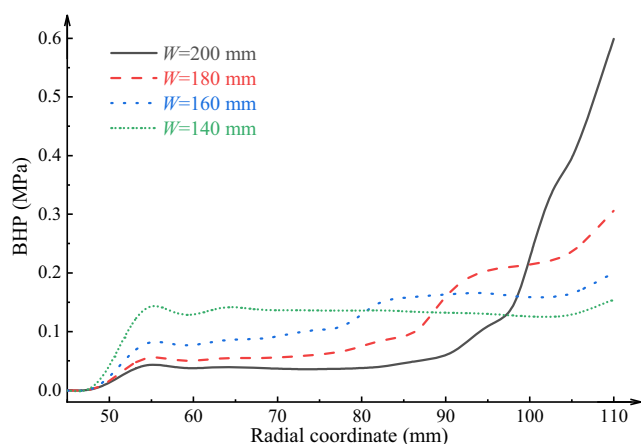


Fig. 22 Schematic diagram of deep drawing. **a** Traditional blank holder technique. **b** ECBH blank holder technique

7 Discussion and conclusions

Compared to traditional methods, in addition to facilitating the control of BHF, the biggest advantage of the ECBH blank holder technique system is energy saving.

Fig. 22 shows the schematic diagrams using conventional process and ECBH blank holder technique, respectively. As shown in Fig. 22a, the counter force F_c is necessary to maintain BHF. F_c needs to be existed all the time during the deep drawing process, which will consume a lot of energy. This energy can be saved by the new blank holder method as shown in Fig. 22b, in which the magnetic force generated by the cushion is an internal force of the deep drawing equipment. The energy consumed by the counter force F_c can be saved. Also, because the press force F_p in Fig. 22b no longer needs to offset the counter force F_c , it will be much smaller than that using the traditional method as shown in Fig. 22a. That is, the tonnage of the press using the new blank holder technique can be much smaller.

From what has been discussed above, the following conclusions can be drawn:

- (1) A novel ECBH technique was developed, by which BHF can be differently applied both in the radial direction and the circumferential direction. Since each piece of the blank holder can be effectively and independently acted on the different flange regions, the deformed metals can be effectively suppressed.
- (2) Since no current exists when BHF is constant, obstacles such as overheating and high energy consumption are no longer a problem. The temperature rises and the generated magnetic force of MEs have been verified by simulation and test, respectively.
- (3) An experimental comparison of the ECBH technique with the single blank holder is given. It was concluded

that the forming ability of the square box can be improved by using the blank holder segmented both in radial and circumferential directions.

- (4) The segmental blank holder technique without the influence of magnetic force is further analyzed by independent simulation and experiment. The forming effective under the action of segmental blank holder technique is much better than that using the traditional method.

Data and materials availability The data sets supporting the results of this article are included within the article.

Author contribution HS Zhang contributed significantly to analysis and manuscript preparation, SJ Qin performed the experiment and contributed to the conception of the study.

Funding The work is supported by the National Natural Science Foundation of China (No. 51675466) and the Natural Science Foundation of Hebei Province of China (No. E2021203043, E2018203373).

Declarations

Ethics approval and consent to participate All authors agree to be signed in the manuscript.

Consent for publication The manuscript is approved by all authors for publication.

Competing interests The authors declare no competing interests.

References

- Ahmetoglu MA, Altan T, Kinzel GL (1992) Improvement of part quality in stamping by controlling blank-holder force and pressure. *J Mater Process Technol* 33(1-2):195–214
- Narayanasamy R, Loganathan C (2006) Study on wrinkling limit of commercially pure aluminium sheet metals of different grades when drawn through conical and tractrix dies. *Mater Sci Eng A-Struct* 419(1/2):249–261
- Obermeyer EJ, Majlessi SA (1998) A review of recent advances in the application of blank-holder force towards improving the forming limits of sheet metal parts. *J Mater Process Technol* 75(1/3):222–234
- Hardt D, Fenn R (1993) Real-time control of sheet stability during forming. *ASME J Eng Ind* 115:299–308
- Endelt B, Tommerup S, Danckert J (2013) A novel feedback control system—controlling the material flow in deep drawing using distributed blank-holder force. *J Mater Process Technol* 213:36–50
- Cheng PY, Chen PJ, Lin YT (2013) Small mechanical press with double-axis servo system for forming of small metal products. *Int J Adv Manuf Technol* 68(9–12):2371–2381
- Modi B, Kumar DR (2013) Development of a hydroforming setup for deep drawing of square cups with variable blank holding force technique. *Int J Adv Manuf Technol* 66(5):1159–1169
- Zhou BJ, Xu YC (2018) The effect of upper sheet on wrinkling and thickness distribution of formed sheet part using double-layer sheet hydroforming. *Int J Adv Manuf Technol* 99:1175–1182
- Siegert K, Doege E (1993) CNC hydraulic multipoint blankholder system for sheet metal forming presses. *CIRP Ann-Manuf Technol* 42(1):319–322
- Lovrec D, Kastrevc M, Ulaga S (2009) Electro-hydraulic load sensing with a speed-controlled hydraulic supply system on forming machines. *Int J Adv Manuf Technol* 41(11–12):1066–1075
- Zhao SD, Zhang ZY, Zhang Y, Yuan JH (2007) The study on forming principle in the process of hydro-mechanical reverse deep drawing with axial pushing force for cylindrical cups. *J Mater Process Technol* 187–188:300–303
- Kriechenbauer S, Mauermann R, Muller P (2014) Deep drawing with superimposed low-frequency vibrations on servo-screw presses. *Proc Eng* 81:905–913
- Qu E, Li M, Li R (2019) Investigation of forming accuracy in multipoint forming with composite elastic pads. *Int J Adv Manuf Technol* 105:4401–4413
- Li H, Wang Q, Fang H, Zheng YY, Sun YQ (2019) Design, numerical simulation, and experimental validation of a novel electromagnetic blank holding system for conventional drawing process. *Int J Adv Manuf Technol* 102:2183–2193
- Seo YR (2008) Electromagnetic blank restrainer in sheet metal forming processes. *Int J Mech Sci* 50(4):743–751
- Lai ZP, Cao QL, Zhang B, Han XT, Zhou ZY, Xiong Q, Zhang X, Chen Q, Li L (2015) Radial Lorentz force augmented deep drawing for large drawing ratio using a novel dual-coil electromagnetic forming system. *J Mater Process Technol* 222:13–20
- Huang YJ, Lai ZP, Cao QL, Han XT, Liu N, Li XX (2019) Controllable pulsed electromagnetic blank holder method for electromagnetic sheet metal forming. *Int J Adv Manuf Technol* 103:4507–4517
- Lai ZP, Cao QL, Han XT, Xiong Q, Deng FQ, Zhang X (2016) Design, implementation, and testing of a pulsed electromagnetic blank holder system. *IEEE Trans Appl Supercon* 26(4):601–605
- Cao QL, Han XT, Lai ZP, Xiong Q, Zhang X, Chen Q, Xiao HX, Li L (2015) Analysis and reduction of coil temperature rise in electromagnetic forming. *J Mater Process Technol* 225:185–194
- Zienkiewicz OC, Lyness J, Owen DRJ (1977) Three-dimensional magnetic field determination using a scalar potential — a finite element solution. *IEEE Trans Magn* 13(5):1649–1656
- Liang BW, Hu SG (1987) Theory of sheet forming plasticity. China Machine Press, Beijing
- Senior BW (1956) Flange wrinkling in deep-drawing operations. *J Mech Phys Solids* 4(4):235–246
- Hill R (1958) A general theory of uniqueness and stability in elastic-plastic solids. *J Mech Phys Solids* 6(3):236–249
- Qin SJ, Xiong BQ, Lu H, Zhang TT (2012) Critical blank-holder force in axisymmetric deep drawing. *T Nonferrous Metal Soc* 22(S2):239–246

Publisher's note Springer Nature remains neutral with regard to jurisdictional claims in published maps and institutional affiliations.